INTERNATIONAL JOURNAL FOR NUMERICAL METHODS IN FLUIDS, VOL. 13, 49–59 (1991)

A MULTIGRID SOLVER FOR THE VORTICITY–VELOCITY NAVIER–STOKES EQUATIONS

M. NAPOLITANO AND L. A. CATALANO

Istituto di Macchine ed Energetica, Università di Bari, via Re David, 200, I-70125 Bari, Italy

SUMMARY

This paper provides a multigrid incremental line-Gauss–Seidel method for solving the steady Navier–Stokes equations in two and three dimensions expressed in terms of the vorticity and velocity variables. The system of parabolic and Poisson equations governing the scalar components of the vector unknowns is solved using centred finite differences on a non-staggered grid. Numerical results for the two-dimensional driven cavity problem indicate that the spatial discretization of the equation defining the value of the vorticity on the boundary is extremely critical to obtaining accurate solutions. In fact, a standard one-sided three-point second-order-accurate approximation produces very inaccurate results for moderate-to-high values of the Reynolds number unless an exceedingly fine mesh is employed. On the other hand, a compact two-point second-order-accurate discretization is found to be always satisfactory and provides accurate solutions for Reynolds number up to 3200, a target impossible heretofore using this formulation and a non-staggered grid.

KEY WORDS Incompressible flows Vorticity–velocity Navier–Stokes Multigrid

INTRODUCTION

In the last few years the first author has developed robust and efficient numerical schemes for solving the vorticity–stream function Navier–Stokes equations.[1–4] A deferred correction strategy[5] on the discrete equations written in delta form[6] has been combined with a robust multigrid block-line-Gauss–Seidel (BLGS) relaxation procedure to obtain second-order-accurate steady state solutions to rather difficult problems at very low computer costs.[7] A new effort has now been undertaken, aimed at developing a similar numerical method for calculating 3D flows, using the vorticity–velocity equations.

For such a formulation, several studies have already appeared in the literature; see e.g. References 8–18. In most investigations the governing equations have been written as a system of parabolic and Poisson equations for each component of the vorticity and velocity vectors. According to this kind of approach, the conditions that the velocity field is divergence-free, its curl equals the vorticity and, in the 3D case, the vorticity vector field too is divergence-free are left aside from the set of governing equations and therefore there is no guarantee that their discrete form be satisfied. In practice, in 2D problems, a spatial discretization based on a staggered grid is found to satisfy these conditions; see e.g. References 12 and 14, which provide accurate high-*Re* solutions for reasonable values of the mesh size. On the contrary, if one uses standard (i.e. non-staggered) finite differences, the numerical solution does not satisfy the discrete counterparts of these conditions exactly and is very sensitive to the discretization of the equation used to evaluate the vorticity at solid walls.[10] As a consequence, no standard finite difference solution to the

0271–2091/91/110049–11$05.50
© 1991 by John Wiley & Sons, Ltd.
Received August 1989
Revised July 1990

vorticity–velocity equations has been reported to date for $Re > 1000$. For example, References 9 and 10 provide only low-Re results, despite the fact that a very accurate exponential scheme[9] and a third-order-accurate upwind approximation[10] have been used for the discretization of the advection term; similarly, a non-uniform grid with 51×51 points has been necessary in Reference 11 to obtain the solution at $Re = 1000$.

For the 3D formulation the situation is even worse. In fact, a standard finite difference method does not satisfy any of the three aforementioned conditions, whereas the solution calculated using a staggered grid provides a divergence-free velocity field but a vorticity field which is neither divergence-free nor equal to the curl of the velocity.[18] To date, staggered-grid solutions which satisfy the discrete form of all three conditions exactly have been obtained only using a so-called div–curl formulation[13] in which the continuity equation and the definition of the vorticity are taken as a system of first-order equations governing the velocity, in place of the Poisson equations.

It therefore appears interesting and worthwhile to address the following questions. (i) Is a standard finite difference discretization of the vorticity–velocity equations viable at high values of the Reynolds number? (ii) For the 3D case, could the Poisson equations for the velocity components still be used (on a staggered grid) while assuring the solenoidal character of the vorticity field and its correct relationship to the velocity? Whereas this second question has been addressed in a parallel effort,[18] the first one is the main object of this paper.

In a preliminary study[16] a node-centred incremental BLGS method has been developed for the 2D vorticity–velocity equations and applied to solve the driven cavity flow problem at $Re \leq 1000$. The solutions were found to be much more sensitive to the treatment used for evaluating the vorticity at solid walls than one would have anticipated from References 10–12. A one-sided two-point first-order-accurate discretization of the vorticity definition at solid boundaries produced very inaccurate results already at $Re = 100$; a three-point one sided second-order-accurate discretization produced accurate results at $Re = 100$ but very inaccurate ones at $Re = 1000$; finally, two different two-point compact discretizations produced reasonably accurate results at both values of the Reynolds number; see Reference 16 for more details. That study, however, demonstrated that the method was not efficient enough to obtain very-fine-grid solutions for $Re = 1000$ or higher at reasonable computer costs. In this paper a scalar version of the method of Reference 16 has been developed and combined with the multigrid strategy of Reference 3, leading to an efficiency gain over the BLGS method of Reference 16 of more than one order of magnitude. Therefore, for the 2D case, the critical issue of the influence on accuracy of the numerical treatment for the vorticity on the boundary can now be addressed for fine enough grids and high enough values of Re within rather limited computer resources. Furthermore, for the 3D case, a rather simple computer code can be built so as to verify the possibility of combining a 3D scalar LGS method with the multigrid strategy of Reference 3 and to assess the computational effectiveness of the resulting numerical scheme.

GOVERNING EQUATIONS

The non-dimensional vorticity transport equation for incompressible viscous flows is given as

$$\partial\omega/\partial t + (\mathbf{V}\cdot\nabla)\omega - (\omega\cdot\nabla)\mathbf{V} = \nabla^2\omega/Re, \tag{1}$$

where ω is the vorticity vector, $\mathbf{V}$ the velocity, ∇ the gradient operator, ∇^2 the Laplacian operator and Re the Reynolds number. Of course the vorticity is defined in terms of the velocity through the relationship

$$\omega = \nabla \times \mathbf{V}. \tag{2}$$

In order to obtain a second-order equation for the velocity, one takes the curl of equation (2). Using the vector identity

$$\nabla\times(\nabla\times\mathbf{V})=\nabla(\nabla\cdot\mathbf{V})-\nabla^2\mathbf{V} \tag{3}$$

and the incompressibility constraint

$$\nabla\cdot\mathbf{V}=0, \tag{4}$$

one finally obtains a vector Poisson equation, namely

$$\nabla^2\mathbf{V}=-\nabla\times\boldsymbol{\omega}. \tag{5}$$

The governing equations of interest here are therefore the two vector equations (1) and (5) for the two vector unknowns $\boldsymbol{\omega}$ and $\mathbf{V}$.

As far as the boundary conditions are concerned, $\mathbf{V}$ is prescribed at the solid boundaries, whereas no specification for the tangential components of $\boldsymbol{\omega}$ is in general available. On the other hand, the two unknown variables $\boldsymbol{\omega}$ and $\mathbf{V}$ must be such that the mutual relationship (2) and the continuity equation (4) be satisfied.

The missing boundary conditions for $\boldsymbol{\omega}$ could be obtained by enforcing at solid boundaries either equation (2)[9-12,14,16-18] or the continuity equation (4) together with the tangential components of the vorticity definition (2), namely[15]

$$\mathbf{n}\times\boldsymbol{\omega}=\mathbf{n}\times(\nabla\times\mathbf{V}), \tag{6}$$

where $\mathbf{n}$ is the unit vector normal to the solid boundary.

The vorticity definition (2) provides very simple expressions for the unknown values of the vorticity at the boundary in both 2D and 3D and therefore is used to complete the formulation of the differential problem in this study.

In conclusion, for Cartesian co-ordinates, the governing equations (1) and (5) are given as

$$\omega1_t+V1\omega1_x+V2\omega1_y+V3\omega1_z-V1_x\omega1-V1_y\omega2-V1_z\omega3=(\omega1_{xx}+\omega1_{yy}+\omega1_{zz})/Re, \tag{7}$$

$$\omega2_t+V1\omega2_x+V2\omega2_y+V3\omega2_z-V2_x\omega1-V2_y\omega2-V2_z\omega3=(\omega2_{xx}+\omega2_{yy}+\omega2_{zz})/Re, \tag{8}$$

$$\omega3_t+V1\omega3_x+V2\omega3_y+V3\omega3_z-V3_x\omega1-V3_y\omega2-V3_z\omega3=(\omega3_{xx}+\omega3_{yy}+\omega3_{zz})/Re, \tag{9}$$

$$V1_{xx}+V1_{yy}+V1_{zz}=\omega2_z-\omega3_y, \tag{10}$$

$$V2_{xx}+V2_{yy}+V2_{zz}=\omega3_x-\omega1_z, \tag{11}$$

$$V3_{xx}+V3_{yy}+V3_{zz}=\omega1_y-\omega2_x. \tag{12}$$

In equations (7)–(12), $V1$, $V2$, $V3$ and $\omega1$, $\omega2$, $\omega3$ are the three Cartesian components of $\mathbf{V}$ and $\boldsymbol{\omega}$ respectively, x, y, z are the Cartesian co-ordinates and subscripts indicate partial derivatives.

As far as the numerical boundary conditions are concerned, the three velocity components are prescribed at all solid boundaries and the three vorticity components are given from equation (2), namely

$$\omega_1=V3_y-V2_z, \tag{13}$$

$$\omega2=V1_z-V3_x, \tag{14}$$

$$\omega3=V2_x-V1_y. \tag{15}$$

In the present study only the 2D and 3D driven cavity flows will be considered; see Figures 1 and 2. In both cases, in equations (13)–(15) only the derivatives normal to the solid walls are different from zero.

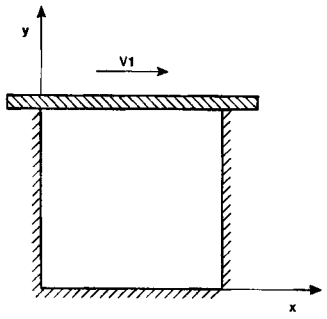

Figure 1. 2D driven cavity flow geometry

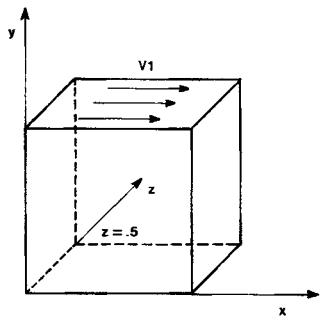

Figure 2. 3D driven cavity flow geometry

NUMERICAL METHOD

Equations (7)–(12) are discretized and linearized in time using a two-level implicit Euler scheme and the delta form of Beam and Warming.[16] Here only the first components of equations (3) and (5), namely equations (7) and (10), will be considered for brevity:

$$\Delta\omega 1/\Delta t + V1\Delta\omega 1_x + V2\Delta\omega 1_y + V3\Delta\omega 1_z - V1_x\Delta\omega 1 - (\Delta\omega 1_{xx} + \Delta\omega 1_{yy} + \Delta\omega 1_{zz})/Re$$
$$= -(V1\omega 1)_x - (V2\omega 1)_y - (V3\omega 1)_z + V1_x\omega 1 + V1_y\omega 2 + V1_z\omega 3$$
$$+ (\omega 1_{xx} + \omega 1_{yy} + \omega 1_{zz})/Re \tag{16}$$

$$\Delta V1/\Delta t - \Delta V1_{xx} - \Delta V1_{yy} - \Delta V1_{zz} = V1_{xx} + V1_{yy} + V1_{zz} - \omega 2_z + \omega 3_y. \tag{17}$$

In equations (16) and (17), $V1$, $V2$, $V3$, $\omega 1$, $\omega 2$, $\omega 3$ refer to the solution at a given iteration level and $\Delta V1$, $\Delta V2$, $\Delta V3$, $\Delta\omega 1$, $\Delta\omega 2$, $\Delta\omega 3$ indicate the unknowns, namely the variations of the dependent variables from the old to the new iteration level. Also, a relaxation-like time derivative has been added to the Poisson equation (10) to parabolize it. Equations (16) and (17) are solved by means of a very robust alternating direction line-Gauss–Seidel method very similar to that of Reference 16. However, here, in each equation, only a single unknown is dealt with implicitly, (e.g., only $\Delta\omega_1$ and its derivatives appear in the left-hand side of equation (16)) the other five variables being evaluated explicitly. In this way each incremental unknown is made independent of the others, so that only scalar tridiagonal systems are solved instead of block tridiagonal ones as in References 2 and 16. It is noteworthy that: (i) the equations on the right-hand sides are the steady state equations, which are discretized using central differences and the conservative form of the advection terms, for accuracy; (ii) first-order-accurate upwind differences are used for the advection terms on the left-hand side of the vorticity transport equations; in this way a 'transient' artificial viscosity is introduced which vanishes as the steady state is reached, while the diagonal dominance of the tridiagonal systems to be solved is guaranteed at all values of Re.[1–5,7]

In order to describe the multigrid procedure employed in this study,[3,4] equations (16) and (17) are rewritten in a more general form by introducing superscripts H and h to indicate the current and the finest grids used in the computations respectively:

$$\Delta\omega 1^H/\Delta t + V1^h\Delta\omega 1_x^H + V2^h\Delta\omega 1_y^H + V3^h\Delta\omega 1_z^H - V1_X^h\Delta\omega 1^H - (\Delta\omega 1_{xx}^H + \Delta\omega 1_{yy}^H + \Delta\omega 1_{zz}^H)/Re$$
$$= C_h^H[-(V1\omega 1)_x - (V2\omega 1)_y - (V3\omega 1)_z + V1_x\omega 1 + V1_y\omega 2 + V1_z\omega 3$$
$$+ (\omega 1_{xx} + \omega 1_{yy} + \omega 1_{zz})/Re]^h, \tag{18}$$

$$\Delta V1^H/\Delta t - \Delta V1_{xx}^H - \Delta V1_{yy}^H - \Delta V1_{zz}^H = C_h^H(V1_{xx} + V1_{yy} + V1_{zz} - \omega 2_z + \omega 3_y)^h. \tag{19}$$

In equations (18) and (19), C_h^H indicates the full-weighting collection operator, applied as many times as needed to go from the finest mesh h to the current mesh H. Starting from an arbitrary initial condition, equations (18) and (19) and the other ones for the remaining vorticity and velocity components are solved on the finest grid h — where they coincide with equations (16) and (17) — by means of a three-sweep (two-sweep for the 2D case) alternating direction LGS iteration, to provide $\Delta\omega 1^h$, $\Delta V1^h$, etc.; the solution ($\omega 1^h$, $V1^h$, etc.) is updated and equations (18) and (19) are solved on successively coarser grids ($H=2h$, $4h$ and $8h$); the entire process is repeated until the finest-grid residual is reduced to a suitably small value. In more detail, at every grid level H the following steps are required: (a) the coefficients on the left-hand side of equations (18) and (19) are injected at the H-mesh grid points using the finest-grid solution ($\omega 1^h$, $V1^h$, etc.) locally, whereas the right-hand side steady state residuals are collected from the finest grid h up to the current grid H; (b) equations (18) and (19) are then solved approximately, using a single sweep of the aforementioned LGS smoother and homogeneous Dirichlet boundary conditions, to provide $\Delta\omega 1^H$, $\Delta V1^H$, etc.; (c) $\Delta\omega 1^h$, $\Delta V1^h$, etc. are evaluated as

$$(\Delta\omega 1^h, \Delta V1^h, \text{etc.}) = I_H^h(\Delta\omega 1^H, \Delta V1^H, \text{etc.}), \tag{20}$$

where I_H^h is the standard multilinear interpolation operator from the current grid H to the finest grid h; (d) the finest-grid solution is updated as

$$(\omega 1^h, V1^h, \text{etc.}) = (\omega 1^h, V1^h, \text{etc.}) + (\Delta\omega 1^h, \Delta V1^h, \text{etc.}); \tag{21}$$

(e) the vorticity at the boundary is finally corrected so as to satisfy equation (2) (i.e. equations (13)–(15)) on the finest mesh. For the 2D case, all steps are performed twice, with the LGS solution method marching from left to right and from top to bottom of the computational domain respectively. For the 3D case the same steps are performed three times, the LGS solution method marching from backwards to forwards in the third sweep. The multigrid cycle is shown schematically in Figure 3, where it is seen to differ from the more usual V, W and sawtooth cycles; see References 3 and 4 for more details.

A detailed discussion of the spatial discretization used for equations (13)–(15) is in order. In Reference 16, for the 2D driven cavity problem, using uniform grids with $h \geq 1/40$, it was found that: a first-order-accurate approximation of equation (15) produced very inaccurate results already at $Re=100$; the standard one-sided second-order-accurate discretization became inadequate at $Re=1000$; two second-order-accurate compact approximations were satisfactory at both values of Re. Here, in order to conduct a more thorough analysis, only two second-order-accurate discretizations of equation (15) are considered, for consistency with the order of accuracy at internal grid points. Therefore, with reference to Figure 4 and assuming $V2=$ constant on the

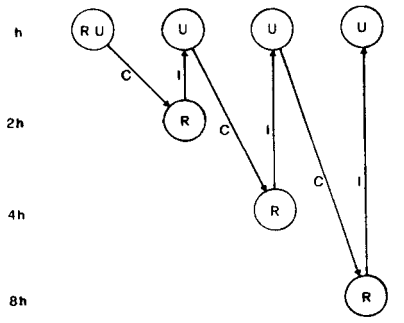

Figure 3. Scheme of the multigrid cycle: R, relaxation; U, updating; C, collection; I, interpolation

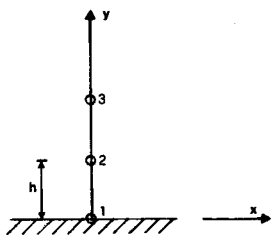

Figure 4. Near-wall grid point distribution

wall, the following discrete forms of the equation $\omega 3 = V2_x - V1_y = -V1_y$, for example, are employed:

$$\omega 3_1 = (V1_3 - 4V1_2 + 3V1_1)/2h, \tag{22}$$

$$\omega 3_1 = -\omega 3_2 - 2(V1_2 - V1_1)/h. \tag{23}$$

Equation (22) is obviously second-order-accurate. In equation (23) the term $V2_{x,2}$ which should have to appear on the right-hand side has been neglected. In fact,

$$V2_{x,2} = V2_{x,1} + V2_{xy,1}h + O(h^2) \tag{24}$$

and, from the continuity equation at the grid point 1 on the solid wall,

$$V2_{xy,1} = -V1_{xx,1} - V3_{zx,1}. \tag{25}$$

Now, $V2_{x,1}$, $V1_{xx,1}$ and $V3_{zx,1}$ are all zero, so that $V2_{x,2}$ is also zero within second-order accuracy.

For the 3D case, symmetry allows one to halve the computational domain (see Figure 2). Therefore different boundary conditions are needed on the symmetry plane ($z = 0{\cdot}5$): $\omega 1$, $\omega 2$ and $V3$ are set to zero; $\omega 3$ is computed from equation (15), with $V2_x$ and $V1_y$ being approximated using standard central differences; $V1$ and $V2$ are evaluated from the corresponding Poisson equations (10) and (11), discretized using central differences. The additional unknowns at the image points outside the computational domain are eliminated by means of the appropriate derivative symmetry or antisymmetry conditions, again discretized by means of standard central differences.

2D RESULTS

The classical driven cavity flow problem[19] was considered in this study; see Figure 1. The efficiency of the present method was addressed at first, by computing the solution for $Re = 100$ on a uniform grid with $h = 1/48$ and the solution for $Re = 1000$ on a uniform grid with $h = 1/96$. The convergence histories are given in Figure 5 and 6 respectively, where the logarithm of the residual of the vorticity equation (R) is plotted versus the work (W). One work unit is the CPU time

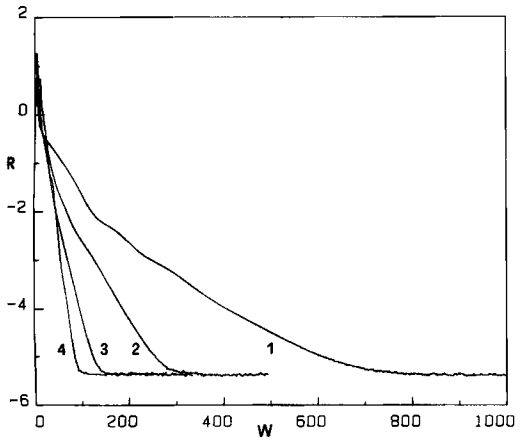

Figure 5. Convergence history for $Re = 100$, $h = 1/48$

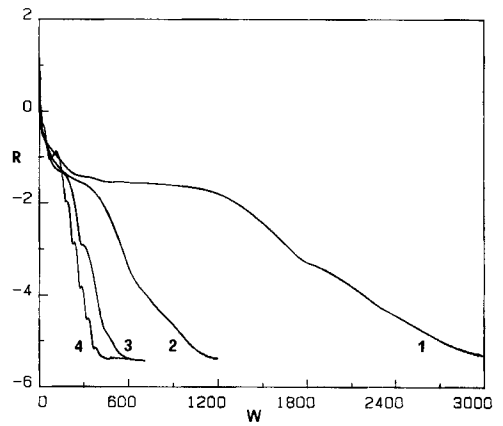

Figure 6. Convergence history for $Re = 1000$, $h = 1/96$

required to perform a two-sweep (alternating direction) LGS iteration on the finest grid. The results corresponding to using one, two, three and four grid levels are given in the figures. The efficiency improvement due to the use of multiple grids is remarkable, the four-grid method converging to machine zero in about seven to eight times less work than the basic smoother using a single grid in both cases. Obviously, for $Re = 1000$ the method converges less rapidly owing to both the higher value of Re and the finer grids used in the calculation. For this case, machine zero on an HP 840S computer using single-precision arithmetic is reached after about 3000 work units when using only the finest grid, but after only about 400 work units when using four grid levels. Incidentally, one work unit for the $h = 1/96$ grid corresponds to about 3 CPU seconds on the aforementioned computer, so that the four-grid computation, carried out to machine zero, requires only about 20 CPU minutes. All these calculations were performed using equation (23) for evaluating the vorticity at solid boundaries and a non-optimized unitary time step.

A simple and efficient method for solving the 2D steady state vorticity–velocity Navier–Stokes equations on a node-centred grid being available, numerical experiments have been conducted to investigate the influence of the two different approximations used to evaluate the wall vorticity, equations (22) and (23). For $Re = 100$ the $h = 1/48$ results are given in Figure 7 as the $V1$ and $V2$ velocity components along the vertical and horizontal centrelines of the cavity. The solid lines show the staggered grid solution of Reference 17. Such a solution satisfies the discrete form of the continuity equation exactly and coincides with that obtained by solving the vorticity–stream function equations on the same grid,[14] so that it can be considered as the best possible second-order-accurate finite difference solution. The broken and dotted lines indicate instead the present results obtained using equations (23) and (22) respectively. Both solutions appear to be satisfactory for this low Reynolds number. A totally different conclusion arises from the $Re = 400$, $h = 1/48$ results given in Figure 8. Whereas the equation (23) results are very similar to the reference solution, the equation (22) results are very inaccurate. It must be pointed out that this solution is converged to machine zero and that the same solution is obtained even if the equation (23) results are used as initial condition for the computer code implementing equation (22). Therefore one can presume that at higher values of Re a much finer mesh is warranted to obtain reasonably accurate results in conjunction with equation (22). In order to verify this hypothesis, the numerical solutions for $h = 1/96$ and $1/192$ have been obtained and are given in Figures 9 and 10 respectively. It clearly appears that the broken lines, indicating the equation (23) results, practically coincide with the solid lines (staggered grid results). The equation (22) results

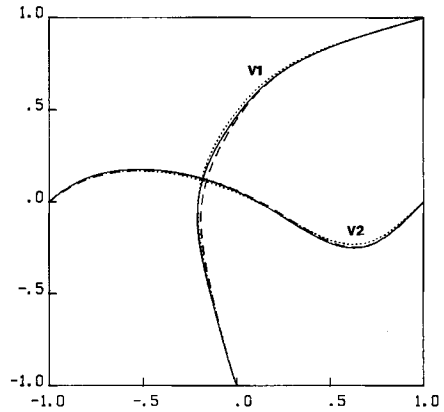

Figure 7. Velocity profiles for $Re = 100$, $h = 1/48$

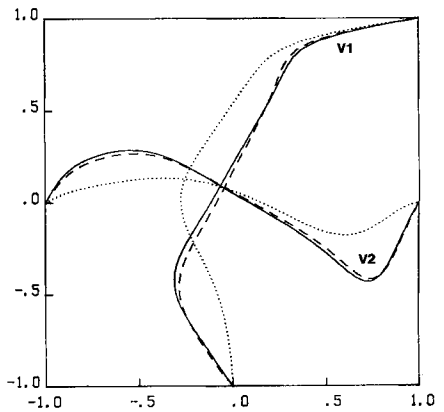

Figure 8. Velocity profiles for $Re = 400$, $h = 1/48$

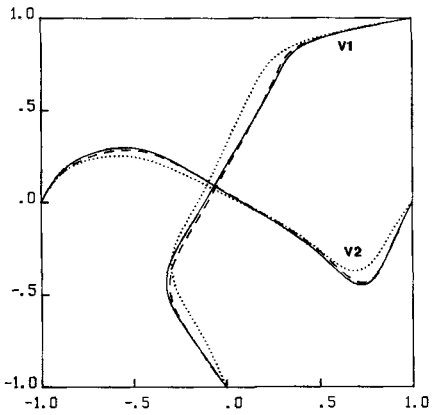

Figure 9. Velocity profiles for $Re=400$, $h=1/96$

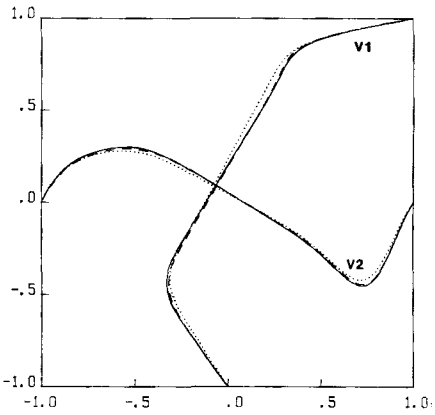

Figure 10. Velocity profiles for $Re=400$, $h=1/192$

instead tend to the reference solution when the mesh is refined but are still remarkably inaccurate for the rather fine $h=1/96$ grid. This fact is disappointing, considering that the solutions provided by the other two methods vary very little when going from the coarsest ($h=1/48$) to the finest ($h=1/192$) mesh.

Needless to say, for the higher value of Re, namely $Re=1000$, the equation (22) results with $h=1/96$ are much less accurate than the corresponding results for $Re=400$ using the same grid; see Figure 11, which provides the usual three sets of solutions. At this point no further mesh refinement was attempted insofar as a very clear conclusion emerges. A second-order-accurate node-centred solution of the vorticity–velocity equations has the same level of accuracy as the corresponding staggered grid solution only if equation (23) is used (instead of equation (22)) to evaluate the vorticity at solid walls. On the contrary, if one uses equation (22), an exceedingly fine mesh is necessary to obtain reasonably accurate results at moderate-to-high values of the Reynolds number. Of course, it would be interesting to understand the basic reason for such a behaviour, which, so far, has escaped the efforts of the authors.

Finally, the more difficult problem with $Re=3200$ was considered using a uniform grid with $h=1/128$ in order to verify the adequacy of equation (23) for such a high value of Re. For this case the present multigrid scheme started to face convergence difficulties and the time step for the vorticity transport equation had to be reduced to 0·2 in order to avoid divergent behaviour. The solution, converged to machine zero within a few CPU hours, is given in Figure 12. Once more, the equation (23) results are acceptable and very similar to the reference staggered grid results of Reference 17.

3D RESULTS

For the 3D driven cavity problem[10] (see Figure 2) only equation (23) has been employed to approximate the numerical boundary conditions given by equations (13)–(15). Only the flows for $Re=100$ and 400 have been considered, higher values of Re requiring excessive CPU time. The numerical results are provided as the longitudinal velocity profile $V1(y)$ at $x=z=0{\cdot}5$. Figure 13 gives the results for $Re=100$. The broken line corresponds to the present node-centred results, obtained using a uniform step size $h=1/32$. The solid line provides the staggered grid results of Reference 18 with $h=1/30$, whereas the circles give the results of Reference 9 with $h=1/25$. Figure 14 gives the results for $Re=400$. The broken and solid lines refer to the present node-

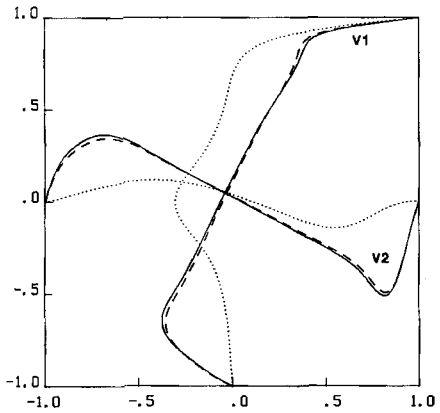

Figure 11. Velocity profiles for $Re = 1000$, $h = 1/96$

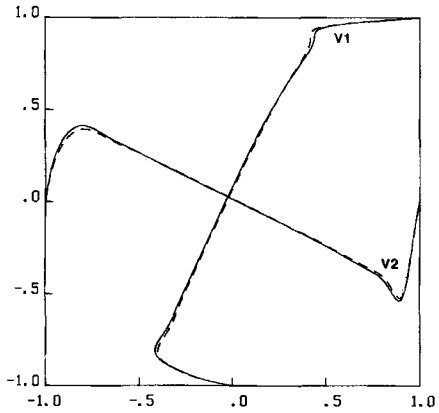

Figure 12. Velocity profiles for $Re = 3200$, $h = 1/128$

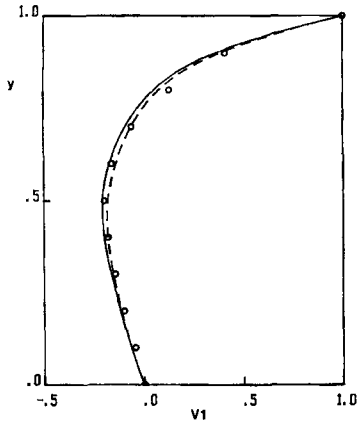

Figure 13. Velocity profiles for 3D flow at $Re = 100$

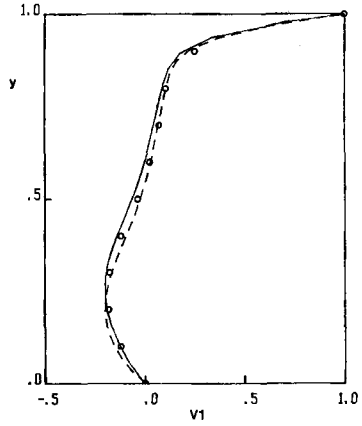

Figure 14. Velocity profiles for 3D flow at $Re = 400$

centred results with $h = 1/32$ and the staggered grid solutions of Reference 18 with $h = 1/24$ respectively, and the circles indicate the $h = 1/20$ solution of Reference 10. From these figures the adequacy of a node-centred discretization combined with the compact discretization used to evaluate the vorticity at solid boundaries is confirmed also for the 3D formulation, at least for moderate values of Re.

It was mentioned that the 3D version of this method was developed to assess the effectiveness of the multigrid strategy of Reference 3 on a 3D scalar line-Gauss–Seidel procedure. The convergence history for $Re = 100$ is given in Figure 15. The solid lines refer to the $h = 1/32$ results and the broken lines to the $h = 1/20$ results. The logarithm of the average residual of the three vorticity components (R) is plotted versus the work (W). The CPU saving obtained in going from one to two grid levels is about one-half, but there is basically no further gain when using three grid levels. This is probably due to the rather coarse (finest) grid used in these 3D calculations. The $Re = 100$ and 400 calculations required about two and twenty CPU hours to converge to machine zero respectively. For $Re = 400$ the time step for the vorticity transport equations had to be reduced from 1·0 to 0·05. Therefore higher values of Re were not attempted.

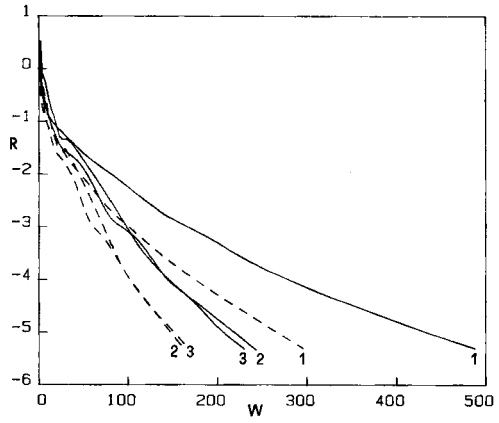

Figure 15. Convergence history for 3D flow at $Re = 100$

CONCLUSIONS

A simple multigrid line-Gauss–Seidel method has been developed for the vorticity–velocity Navier–Stokes equations in two and three dimensions using a non-staggered grid and second-order-accurate central differences. Extensive numerical experiments for the 2D driven cavity flow problem have shown the crucial importance of choosing a particular discretization for the equation used to evaluate the vorticity at solid walls. For the first time, accurate solutions have been obtained using a non-staggered grid vorticity–velocity approach for *Re* as high as 3200. The method has also been proven to be effective for the simple driven cavity problem in 3D, but only at moderate values of the Reynolds number. The simple multigrid strategy employed in this study has provided an efficiency gain of seven to eight times in 2D and of only twice in 3D.

ACKNOWLEDGEMENTS

This research has been supported by MURST and CNR. Some 2D results of this work were presented by the first author at the 4th Copper Mountain Conference on Multigrid Methods, 9–14 April 1989. The authors are indebted to Professor L. Quartapelle for many valuable suggestions and comments.

REFERENCES

1. M. Napolitano, 'Efficient ADI and spline ADI methods for the steady-state Navier–Stokes equations' *Int. j. numer. methods fluids*, **4**, 1101–1115 (1984)
2. M. Napolitano and R. W. Walters, 'An incremental block–line-Gauss–Seidel method for the Navier–Stokes equations', *AIAA J.*, **24**, 770–776 (1986).
3. M. Napolitano, 'An incremental multigrid strategy for the fluid dynamic equations', *AIAA J.*, **24**, 2040–2042 (1986).
4. J. H. Morrison and M. Napolitano, 'Efficient solutions of two-dimensional incompressible steady viscous flows', *Comput. Fluids*, **16**, 119–132 (1988).
5. P. K. Khosla and S. G. Rubin, 'A diagonally dominant second-order-accurate implicit scheme', *Comput. Fluids*, **2**, 207–209 (1974).
6. R. M. Beam and R. F. Warming, 'An implicit factored scheme for the compressible Navier–Stokes equations', *AIAA J.*, **16**, 393–402 (1978).
7. M. Napolitano, 'Efficient solution of two-dimensional incompressible steady separated flows', *Comput. Fluids*, to appear.
8. H. Fasel, 'Investigation of the stability of boundary layers by a finite-difference model of the Navier–Stokes equations', *J. Fluid Mech.*, **78**, 355–383 (1976).

9. S. C. R. Dennis, D. B. Ingham and R. N. Cook, 'Finite-difference methods for calculating steady incompressible flows in three dimensions', *J. Comput. Phys.*, **33**, 325–339 (1979).
10. R. K. Agarwal, 'A third-order-accurate upwind scheme for Navier–Stokes solutions in three dimensions', presented at *ASME Winter Annual Meeting*, Washington, DC, 15–20 November 1981.
11. B. Farouk and T. Fusegi, 'A coupled solution of the vorticity–velocity formulation of the incompressible Navier–Stokes equations', *Int. j. numer. methods fluids*, **5**, 1017–1034 (1985).
12. P. Orlandi, 'Vorticity–velocity formulation for high *Re* flows', *Comput. Fluids*, **15**, 137–150 (1987).
13. G. A. Osswald, K. N. Ghia and U. Ghia, 'A direct algorithm for solution of incompressible three-dimensional unsteady Navier–Stokes equations', *Proc. AIAA 8th Computational Fluid Dynamics Conf.*, Honolulu, HW, June 1987, AIAA, New York, 1987, pp. 408–421.
14. G. Guj and T. Stella, 'Numerical solutions of high *Re* recirculating flows in vorticity–velocity form', *Int. j. numer. methods fluids*, **8**, 405–416 (1988).
15. M. D. Gunzburger and J. S. Peterson, 'On finite element approximations of the stream function–vorticity and velocity–vorticity equations', *Int. j. numer. methods fluids*, **8**, 1229–1240 (1988).
16. P. Giannattasio and M. Napolitano, 'Numerical solutions to the Navier–Stokes equations in vorticity–velocity form', *Proc. Third Italian Meeting of Computational Mechanics*, Palermo, 7–10 June 1988, pp. 95–101.
17. M. Napolitano and G. Pascazio, 'A multigrid LGS method for the vorticity–velocity Navier–Stokes equations', *Notes Numer. Fluid Mech.*, **29**, 430–435 (1990).
18. M. Napolitano and G. Pascazio, 'A numerical method for the vorticity–velocity Navier–Stokes equations in two and three dimensions', *Comput. Fluids.*, to appear.
19. O. R. Burggraf, 'Analytical and numerical studies of the structure of steady separated flows', *J. Fluid Mech.*, **24**, 113–151 (1966).